

#### Contents lists available at ScienceDirect

# Materialia

journal homepage: www.elsevier.com/locate/mtla



# Twinning pathways enabled by precipitates in AZ91

Brandon Leu<sup>a,\*</sup>, M. Arul Kumar<sup>b</sup>, Kelvin Y. Xie<sup>c</sup>, Irene J. Beyerlein<sup>a,d</sup>

- <sup>a</sup> Materials Department, UC Santa Barbara, Santa Barbara, CA 93106, USA
- <sup>b</sup> Materials Science and Technology Division, Los Alamos National Laboratory, NM 87545, USA
- <sup>c</sup> Department of Materials Science and Engineering, Texas A&M University, College Station, TX 77843, USA
- <sup>d</sup> Department of Mechanical Engineering, UC Santa Barbara, Santa Barbara, CA 93106, USA



ARTICLE INFO

Keywords: Magnesium alloy Tensile twin Basal precipitate Local stresses Crystal plasticity

#### ABSTRACT

While precipitates have been shown to substantially strengthen magnesium alloys by blocking the glide of dislocations inside the grain, the interactions between these precipitates and deformation twins, which commonly occur in these alloys, are much less understood. In this work, an elasto-viscoplastic fast-Fourier-transform (EVP-FFT) model is used to study the interactions between plate-shaped basal precipitates and propagating {1012} tensile twins in AZ91 Mg alloy. The results suggest that while precipitates may impede the propagation and thickening of twins, they can also cause stress localizations that can promote the formation of multiple new twins of the same or different crystallographic variants. We show that the location of the twin-precipitate interaction site, whether precipitate-central or precipitate-edge impingement, and the thickness of the precipitate can influence the propensity for twins to expand around the precipitate or nucleate a new twin on the other side of it. Depending on the twin-precipitate impingement site, we propose multiple twinning pathways that can help explain how twins can proliferate in the magnesium alloys in the presence of precipitates.

## 1. Introduction

Magnesium (Mg) alloys are exceptionally lightweight structural metals (density,  $\rho \sim 1.74~\frac{g}{cm^3}$ ), being approximately 30% lighter than aluminum and 75% lighter than steel. This property alone makes them highly attractive candidates for many structural applications where lighter components can mean greater energy efficiency and lower costs [1,2]. Furthermore, Mg is abundant and recyclable, making it environmentally sustainable [2]. However, many common Mg alloys are not sufficiently strong for typical industrial applications since their tensile yield strengths lie between 80-120 MPa [3,4], far below the tensile yield strength of 350 MPa of high-strength steels [5] and below 100-240 MPa that of most aluminum 6000 series alloys [6]. In order to increase their strengths, various mechanisms have been employed to restrict the motion of dislocation glide in Mg alloys. A recent study showed that Mg alloys containing Zn and Ca can form Guinier-Preston (GP) zones to achieve alloys whose combination of ductility and strength are comparable to aluminum 6000 series alloys [7]. More commonly, precipitates can be dispersed throughout the matrix and grain boundaries that block dislocation slip, leading to reported increases in yield strengths up to 156-324 MPa [8].

A number of studies have been carried out to understand slipprecipitate interactions. It is commonly found that precipitates interact with dislocations by acting as hard non-shearable obstacles that block the motion of the dislocations through the matrix grain [9,10]. Accordingly, the increase in the stress required for plastic flow has been approximated by Orowan looping, where the precipitate size, shape, habit plane and spacing play important roles in determining amount of strengthening provided [11–16]. Alternatively, some studies have investigated shearable precipitates, wherein the precipitate displayed signs of being sheared by impinging dislocations [13,17–19]. Precipitate shearing tends to occur when the shear planes of the precipitate and matrix grain are well aligned, a condition that happens more often for basal a dislocations than non-basal dislocations in Mg alloys [13].

In addition to slip, Mg alloys also commonly deform by twinning [20]. Twinning deformation occurs through the coordinated directional shearing of a subregion of a grain along a particular crystallographic twin plane. The resulting twin domain is reoriented with respect to the parent grain, such that the parent and twin have a mirror symmetry across the twin plane [20]. Twinning introduces sub-grain domains and the associated boundaries in the microstructure, as well as heterogeneous stress and strain fields within and in the vicinity of twin domains [21,22]. In AZ91,  $\{10\bar{1}2\}$  tensile twinning deformation can occur at room temperature and large twin volume fractions up to 35% have been observed by 2% strain [23]. Due to the severe consequences of twinning on the microstructure and local micromechanical fields, the structural properties of Mg alloys are strongly dependent on their twinning behav-

E-mail address: brandonleu@ucsb.edu (B. Leu).

<sup>\*</sup> Corresponding author.

ior. Thus, understanding interactions between twins and precipitates is paramount to designing precipitate-rich Mg alloys with high strength.

In contrast to slip, twin-precipitate interactions have received less attention. Unlike slip, twins are three dimensional domains that form through a sequence of steps, including nucleation, propagation and thickening of the twin domain [20]. The twin-precipitate interactions during each of these steps are unique and important for determining the development of the overall twinned microstructure and mechanical properties of the alloy. In general, experimental studies have found the volume fraction of twins remain consistent, regardless of precipitate volume fractions [24,25]. However, the presence of precipitates correlate well with an increase in the density of twins and a decrease in twin size, implying that precipitates can enhance multiple twin formation while suppressing twin thickening [23,26–28].

Twin-precipitate interactions that involve twin nucleation have been investigated by computational methods. Tang et al. used molecular dynamics (MD) simulations to show that twin-precipitate interaction sites can initiate twinning dislocation loops that lead to a reduction in the resolved shear stress needed to nucleate twinning dislocation partials under strain rates of  $10^6/s$  at 283 K [29]. Using MD simulations, Fan et al. showed that basal dislocations and stacking faults can nucleate at the twin-precipitate interfaces causing local plastic relaxation [30]. As a result, they were able to rank the effectiveness of precipitate shapes on hardening, showing that spheres have the strongest hardening, followed by plates and then rods [30].

A majority of studies in literature investigate twin-precipitate interactions that affect twin thickening, where a distribution of precipitates block the lateral migration of the twin boundary [11,16,29,30]. Some models have been proposed that have treated twinning synonymously with slip and described the strengthening by Orowan bowing of twinning dislocation partials around the precipitates [27,28,31]. Barnett extended this idea by representing the twinning dislocations as a wall of super-dislocations, which yielded closer approximations to experimentally observed values of strengthening [32]. This model was later supported by dislocation-dynamics (DD) simulations [33]. Jain et al. used transmission electron microscopy (TEM) combined with visco-plastic self-consistent modeling to study the role of long-range elastic backstresses developed by precipitates on tensile twins [24]. Liu et al. used crystal plasticity phase-field simulations to show that precipitate size and habit-plane alignment with the twin boundary play critical roles on the resolved shear stress required for twin thickening [16]. Recently, by employing crystal plasticity based finite element method, Siska et al. simulated the twin-precipitate interaction in a Mg alloy to study the effect of precipitates on twin boundary migration [34]. They showed that precipitates can indirectly suppress the twin thickening process by hardening the slip modes that would normally relax stresses around the twin

Unlike twin-precipitate interactions involving the interaction between precipitates and migrating twin boundaries, considerably less studies focus on the effects of interactions of twin-tips and precipitates during propagation. The ability of precipitates to potentially divert, blunt, or aid the nucleation of new twins near the interaction site can affect twinning microstructure (e.g., morphology and variant selection), and the accommodation of plasticity. Understanding how these interactions progress in time is difficult to identify with local post-mortem analyses, especially when information is collected from many different samples. To gain statistically significant information in this regard, most recently Xie et al. [35] investigated the effect of precipitates on different stages of {1012} tensile twinning in a Mg-9 wt.% Al alloy micropillar using precision electron diffraction. They used a sample that contained a heterogeneous distribution of basal type precipitates, facilitating the ability to capture the different stages of twin-precipitates interactions within the same scanned area. In doing so, they were able to isolate twin-precipitate interactions during propagation in a region where twin thickening was limited. They observed that basal-plate precipitates can arrest propagating twin tips but seem to allow new twins to nucleate on the other side of the precipitate. They considered regions in the interior volume of the micropillar in addition to near the surface and found that precipitates tend to promote multiple twin formation, in line with observations reported in the literature [23,26–28].

The focus of the study is to elucidate the interactions between twintips and precipitates that control the microstructural evolution during the propagation stage of twinning. We employ a full-field elasto visco-plastic fast Fourier transform (EVP-FFT) model to calculate the local stress fields around twin/precipitate configurations involving commonly observed basal-type precipitates and the  $\{10\bar{1}2\}$  tensile twin in AZ91 alloy [35,36]. We calculate the twin plane resolved shear stress (TRSS) in the vicinity of the twin boundary, twin tip, and around the precipitates to determine the local driving forces available for different bypass mechanisms and gain some insight into which one is likely to occur. For most cases, we consider the case in which the twin thickness is much finer than the length of the precipitate.

We study the impingement of a single propagating twin near the center and edges of plate-shaped basal precipitates. We find that the thickness of the precipitate, relative to the thickness of the twin, has a strong effect on the likely outcome of the interaction or bypass mechanism. Our findings show that central-impingement is more effective at blocking twin propagation than edge-impingement. In both cases, highly localized twin stresses develop around the impingement site that can serve as sites for new twins to nucleate. These results may help to identify cases in which complex network structures of twins that apparently "cross" precipitates can emerge. To continue propagating, it is not likely that the twin would thicken or migrate around the precipitate but would rather reform on the other side of the precipitate. The effects of relative precipitate thickness on the number, location and variant of twins that can form in this situation are investigated.

#### 2. Numerical methods

#### 2.1. EVP-FFT formulation for twin/precipitate interactions

Crystal-plasticity based elasto-viscoplastic fast Fourier transform (EVP-FFT) model is used here [21,37,38]. The modeling framework was originally developed by Lebensohn et al. to study micromechanical fields in polycrystals [38]. Since then, it has been extended to study multi-phase materials, twinning deformation and free surface relaxation [21,38-41]. In this work, the formation of the precipitates is not simulated; rather, they are predefined domains with appropriate material properties and crystallographic orientations. Subcrystalline twin domains in this model are explicitly formed by rotating the twin domain according to its crystallographic twinning relationship with the parent matrix, and slowly incrementing a twinning shear transformation eigenstrain equal to the characteristic twin shear. During this process of creating the twin, the boundary conditions are held constant and the simulation cell is relaxed to an energetic minimum after each step. No external loads were applied prior to the formation of the twin to isolate the stress fields arising between a single twin/precipitate interaction. Applying a macroscopic stress of any level is straightforward in the model and would undoubtedly convolute the stress field. External stresses would be important to quantify the level of stress needed to thicken the twin. Yet, before considering such later stages of thickening, we aim to first examine how precipitates can influence the pathway taken by initially propagating twins. Below, we provide a brief review of the EVP-FFT formulation with explicit twin domains is described below.

The solution of an EVP problem is calculated using an appropriate time discretization scheme. Accordingly, the generalized Hooke's law that relates the stress and strain fields at each material point,  $\mathbf{x}$ , is written as:

$$\sigma^{t+\Delta t}(x) = C(x) : \varepsilon^{e,t+\Delta t}(x)$$
 (1)

Here, the superscript  $t + \Delta t$  denotes an increment in time, t, by  $\Delta t$ . In the above equation,  $\sigma(x)$  is the Cauchy stress tensor, C(x) is the elastic

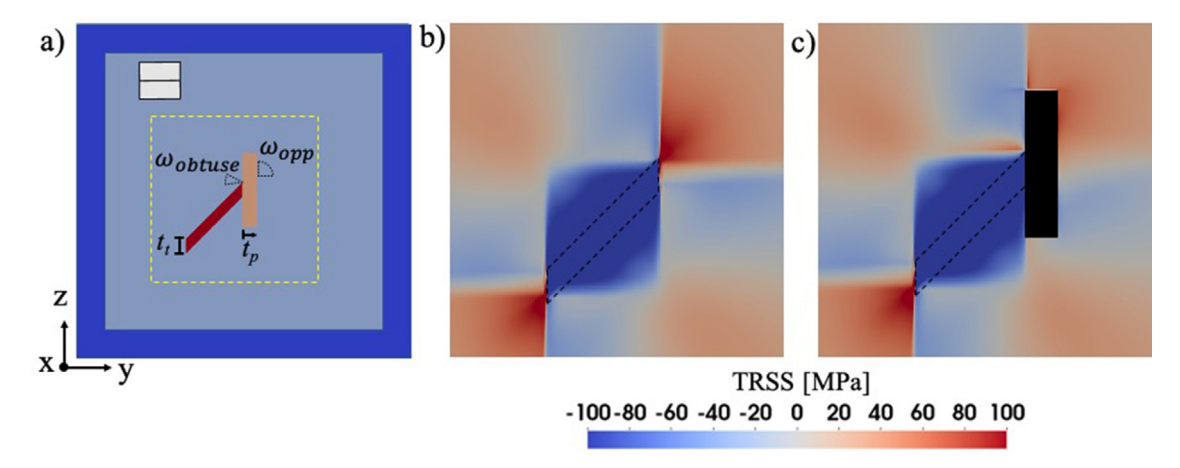


Fig. 1. The calculated TRSS fields without and with a basal-plate  $Mg_{17}Al_{12}$  precipitate. (a) Schematic of the simulation set-up. A polycrystalline buffer layer surrounds the parent grain of AZ91 Mg alloy. The  $Mg_{17}Al_{12}$  precipitate lies on the basal plane of the parent grain with a  $\{10\overline{1}2\}$  tensile twin impinging on it. The orientation of the parent grain is illustrated by the hexagonal inset. Peak TRSS values develop in regions  $\omega_{opp}$  and  $\omega_{obtuse}$  marked with black dotted lines on both sides of the precipitate. (b) The TRSS field when a twin develops without a precipitate nearby. (c) The TRSS field when a twin impinges on a precipitate. The twin boundary is outlined in dashed black lines.

stiffness tensor, and  $\varepsilon^e$  is the elastic strain tensor. Under an infinitesimal strain approximation, the elastic strain tensor can be rewritten as the total strain tensor,  $\varepsilon$ , minus total plastic strain tensor. In this model, the total plastic strain is equal to the sum of the plastic slip strain due to slip,  $\varepsilon^p$ , and the twin shear transformation strain,  $\varepsilon^{tw}$ .

$$\varepsilon^{e,t+\Delta t}(x) = \varepsilon^{t+\Delta t}(x) - \varepsilon^{p,t}(x) - \varepsilon^{p,t+\Delta t}(x)\Delta t - \varepsilon^{tw,t}(x) - \Delta \varepsilon^{tw}(x)$$
 (2)

Here, the plastic strain rate due to slip is constitutively related to the stress tensor via a sum of shear-rates over all the slip systems:

$$\dot{\varepsilon}^{p}(x) = \sum_{s=1}^{N} m^{s}(x) \dot{\gamma}^{s}(x) = \gamma_{o} \sum_{s=1}^{N} m^{s}(x) \left( \frac{|m^{s}(x) : \sigma(x)|}{\tau_{c}^{s}(x)} \right)^{n} sgn(m^{s}(x) : \sigma(x))$$
(3)

where  $\tau_C^S(x)$  is the critical resolved shear stress (CRSS) associated with the slip system s,  $\dot{\gamma}_o$  is a normalization factor, and n is the stress exponent (inverse of the rate-sensitivity exponent). The tensor m is the Schmid tensor, which is the symmetric part of  $(b^s \cdot n^s)$ , and  $b^s$  and  $n^s$  are the unit vectors along the slip direction and the slip plane normal, respectively, of slip system s.

In the twin domain, the shear increment,  $\Delta \varepsilon^{tw}$ , is explicitly incremented over N<sup>tw</sup> steps until the characteristic twin shear,  $g^{tw}$ , is achieved on the twin plane and in the twin shear direction of the selected twin variant. In this work, to ensure numerical convergence the twinning shear is imposed over 2000 N<sup>tw</sup> steps. Note that the  $\varepsilon^{tw}$  and  $\Delta \varepsilon^{tw}$  everywhere outside of the twin domain is zero. The increment in the twin transformation strain is given by,

$$\Delta \varepsilon^{tw} = m^{tw} \frac{g^{tw}}{N^{tw}} \tag{4}$$

where  $m^{tw}$  is the symmetric part of  $(b^{tw} \cdot n^{tw})$ , where  $b^{tw}$  and  $n^{tw}$  are the unit vectors along twin shear and twin plane normal directions, respectively.

## 2.2. Simulation set-up

The simulation size is  $3 \times 600 \times 600$  voxels and consists of a 50-voxel thick buffer layer (dark blue) that encompasses the parent grain. The buffer layer approximates the response of a polycrystalline medium with a uniform distribution of crystal orientations (*i.e.*, random texture), and is sufficiently thick to prevent the micromechanical fields from overlapping due to the periodic boundary conditions. The simulations are designed to elucidate the influence of  $Mg_{17}Al_{12}$  basal precipitates on  $\{10\bar{1}2\}$  tensile twin development within AZ91 alloy. Fig. 1 illustrates the

periodic simulation cell in all simulations, depicting a tensile twin (red) lamella impinging on a  $Mg_{17}Al_{12}$   $\beta$ -phase precipitate (orange) within the center of a parent grain (light blue).

The crystallographic orientation of the parent grain, in the Bunge convention, is (0°, 90°, 0°), which aligns its c-axis with the y-direction. The orientation of the parent grain is represented by the hexagonal inset in the top left, Fig. 1a. Based on the experimental observations, the basal precipitate assumes a thin plate-shape and lies on a habit plane that is parallel to the basal plane of the matrix grain [36,42,43]. The precipitate and the matrix share the Potter orientation relationship, commonly observed in electron microscopy, given by  $(0001)_{\mbox{\scriptsize Mg}}$   $2^{\circ}$  from  $(011)_{\beta}$ ,  $[2\overline{11}0]_{Mg}$  //  $[1\overline{1}1]_{\beta}$ , and  $(01\overline{1}1)_{Mg}$  //  $(110)_{\beta}$  [9,36,43]. Accordingly, the crystallographic orientation of the precipitate for the selected parent grain orientation is given by (39.23°, 114°, 63.43°), in the Bunge convention. The angle of incidence of the twin on the basal precipitate depends on the twin type and its variant. In this work, the variant explicitly simulated is the  $(01\overline{1}2)[0\overline{1}11]$  tensile twin, with both its twin plane normal and twin shear direction lying in the y-z plane. In this way, there is no out-of-plane twinning shear in the x-y and x-z planes, and thus allowing for a 2D model setup and lower computational costs. The selection of another  $\{10\overline{1}2\}$  tensile twin variant or orientation of the precipitate within the Potter orientation relationship is not expected to yield significantly different results.

With periodic boundary conditions, the microstructure is columnar with the cross-section shown in Fig. 1a. While a 3D simulation is possible with the EVP-FFT model, it is not necessary since the simplified 2D microstructure can reasonably approximate the majority of twin-precipitate impingement events. More importantly, the crystallography of the {1012} tensile twin and basal precipitates selected for this work permits simulating the interactions in 2D. Typically, little is known about the twin geometry in the out-of-plane of the viewing surface, as these are not readily described in the literature due to the 2D nature of electron-microscopy-based techniques. For these reasons, the 2D version is valid, with the added benefit of permitting more attention to be paid to the relative size of the twin with respect to the precipitate dimensions in the in-plane direction. The results can be extrapolated in the out-of-plane directions where the relative twin thickness and the out-of-plane dimension of the precipitate would be important.

The twin thickness,  $t_t$ , and precipitate thickness,  $t_p$ , are shown in Fig. 1a. The geometry of the plate-shaped precipitates is such that it is large in two dimensions (z- and x-directions) and can be approximated as infinite in comparison to the thickness of newly propagating twins in this studying. Thus, the simplified 2D model is sufficient, as model-

ing the third infinitely large dimension (x-direction) is not expected to change the trends observed in this work. The small dimension of the precipitate (y-direction) is varied to demonstrate how the precipitate thickness can influence twin propagation. The EVP-FFT formulation does not intrinsically contain any physical length scales, and thus relative sizes between the twin-tip thickness and precipitate thickness are used to correlate with experimentally observed microstructures. We have chosen a twin thickness of 22 voxels and a range of precipitate thicknesses from 3 to 88 voxels, resulting in relative precipitate thicknesses with respect to twin-tip thickness that range from 0.14-4.0. In the micrographs presented in the literature, it can be observed that precipitate thicknesses range from 20-400 nm [9,35,44]. By considering a large precipitate thickness of 400 nm represented by 88 voxels, our simulations would correspond with precipitate thicknesses in the range of 13.6-400 nm and a twin thickness of 100 nm, within reasonable approximations of early-stage twin propagation.

In the calculations that follow, we focus on the interaction of the twin tip with precipitates during twin propagation. Newly formed twins that first propagate across the twin-free grain are usually thin compared to the grain size and plate-shape precipitates. Thus, the twin is more likely to imping somewhere in the central portion of the precipitate away from the edges. Here we consider two general yet distinct situations: central impingement and near-edge impingement.

#### 2.3. Materials

In this work, the material system is the AZ91 Mg alloy containing Mg<sub>17</sub>Al<sub>12</sub> precipitates. AZ91 has a hexagonal close-packed (HCP) crystal structure and the elastic constants  $C_{11},\ C_{12},\ C_{13},\ C_{33}$  and  $C_{44}$  are 59.75, 23.24, 21.7, 61.7 and 16.39 GPa, respectively [45]. The initial CRSS for AZ91 for the prismatic a, basal a and pyramidal-type I c + a slip modes were constant throughout the simulation and set to 100, 35, and 160 MPa, respectively [4]. In this work, only the twinning shear transformation is simulated, with no pre- or post-twin straining. Thus, strain hardening was not considered since it is not expected to significantly influence the twinning shear transformation process and allows for easier interpretation of the twin-precipitate interaction induced micromechanical fields. The Mg<sub>17</sub>Al<sub>12</sub> precipitate has a body-centered cubic (BCC) crystal structure, and the elastic constants C<sub>11</sub>, C<sub>12</sub>, and C<sub>44</sub> are 86.8, 29.0, and 20.0 GPa, respectively [46]. In the simulation, the precipitate is treated as an elastically deforming body. It has been observed experimentally that even when twins fully engulf these precipitates they do not shear or plastically deform [9,47].

## 3. Results and discussion

## 3.1. Precipitate effects on twin stresses

We first study the case in which the twin has impinged on a precipitate and the effect of the precipitate on the local stress state around the twin as a way to infer how a precipitate would affect twin propagation and thickening. When a twin develops inside a crystal, due to the crystallographic reorientation and local shearing imposed by the twin, the twin alters the stress state of the crystal compared to the twin-free state. Fig. 1a shows the twin and a precipitate lying on the basal plane and oriented such that the twin tip would impinge on the center of the precipitate. The precipitate is five times longer than its thickness, and the twin thickness is equal to the thickness of the precipitate.

Fig. 1b and c compare the calculated twinning resolved shear stress (TRSS) fields without and with the precipitate, respectively. This stress component is the stress state projected onto the twin plane along the twinning shear direction to determine the driving force for twin development, including propagation and thickening. A positive TRSS supports twin propagation and thickening, while a negative TRSS acts against it (an anti-twinning stress) [20]. In the precipitate-free case, TRSS of

Table 1 Crystallographic twin shear direction, b, and twin plane normal, n, of the  $\{10\overline{1}2\}$  tensile twin variants. The variants V1a, V2a and V3a are the co-zone variants of variants V1, V2, and V3, respectively.

Twin variants	b	n
V1	[1011]	(1012)
V2*	[0111]	$(01\bar{1}2)$
V3	$1\bar{1}01$	$(\bar{1}102)$
V1a	[1011]	$(\bar{1}012)$
V2a	$[01\bar{1}1]$	$(0\bar{1}12)$
V3a	[1101]	$(1\bar{1}02)$

<sup>\*</sup> Denotes the primary twin variant which is explicitly simulated in this work.

about +100 MPa localize in a small region ahead of the twin tip, favoring twin-tip propagation. Along the twin boundary, however, TRSS of about -125 MPa develop, which hinders twin thickening. Fig. 1c shows that with a hard precipitate, the forward stresses ahead of the twin-tip, in the region  $\omega_{opp}$ , decrease by approximately 25% to  $\sim\!+75$  MPa, compared to the precipitate-free case. Additionally, the high stress region in  $\omega_{opp}$  becomes less localized. The anti-twinning stresses along the twin boundary, however, are similar to the precipitate-free case. With the precipitate, in order for the twin to continue propagation, it would have to reform on the other side of the precipitate. Compared to continued twin-tip propagation without the precipitate, a larger critical stress is clearly required. With the lower driving stress and requirement to reform a new twin in  $\omega_{opp}$  and backstresses along the twin boundary, the precipitate hinders the twin from both propagating and thickening.

In addition to  $\omega_{opp}$ , located on the opposite side of the precipitate from where the twin impinges, another highly localized TRSS is generated in a region at  $\omega_{obtuse}$ , where the twin and precipitate come together at an obtuse angle, shown in Fig. 1a. Here, the TRSS reaches  $\sim$  +65 MPa, compared to -20 MPa in the same region without the precipitate. These results are qualitatively in line with trends observed in recent work by Siska et al. [34], who used Finite Element Methods (FEM) to study tensile twins bounded between basal precipitates in AZ91 alloy. Since the precipitates are elastically deforming bodies that do not twin or shear, twinning in the matrix grain can only continue through the nucleation of a new twin in  $\omega_{opp}$  or  $\omega_{obtuse}$ , or through the thickening of the initial twin [9,12,48]. We discuss these three possibilities below.

#### 3.2. Formation of multiple twin variants

The foregoing TRSS fields correspond to a single twin variant impinging on the precipitate. However, it is also commonly observed that multiple variants can develop in grains of deformed precipitate-strengthened Mg alloys [25,27,35,49]. To analyze the possibility for the formation of multiple variants as a result of the twin/precipitate interaction, we consider the same tensorial stress field generated by the twin lamella and precipitate as before, but calculate TRSS fields corresponding to all six crystallographic {1012} tensile twin variants, see Table 1, where V2 is the primary variant which is explicitly simulated in this work. Each of the twin variants are related to each other by rotation symmetry, and thus, the arbitrary choice of any one of the twin variants as the primary variant would result in equivalent resolved shear stresses among the other five variants. V2 was selected to be the primary twin variant because its twin plane normal and twin shear direction lie in-plane (in the Y-Z plane). The TRSS of each of the six variants, V, is calculated as  $m^V(x)$ :  $\sigma(x)$ , where  $m^V(x)$  is the symmetric part of  $b^V \cdot n^V$ , and  $b^V$ and  $n^V$  are the shear direction and plane normal direction of each twin variant, respectively.

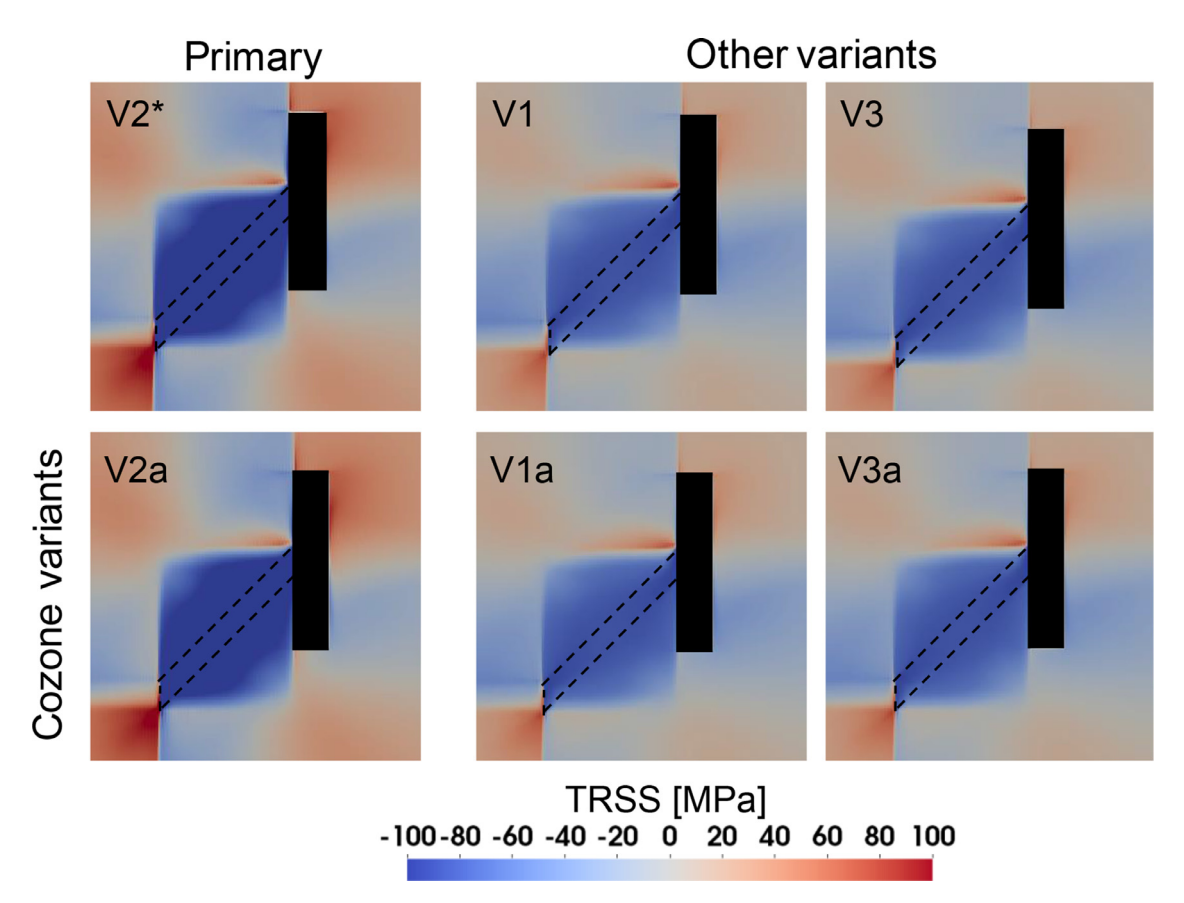


Fig. 2. TRSS fields for three tensile twin variants (top row) and their respective cozone variants (bottom row) due to the impingement of tensile twin variant V2 on a basal plate precipitate. The crystallographic details of these variants are listed in Table 1. \* Denotes the primary twin variant which is explicitly simulated in this work.

Fig. 2 presents these TRSS fields for all six tensile twin variants. The top row shows the TRSS fields for variants V1, V2 and V3 and the bottom row, their respective cozone variants. The TRSS fields of cozone variant pairs (i.e., V2 and V2a) are nearly identical. The TRSS fields of all variants experience qualitatively similar trends to that observed for V2. Among all, twin V2 and its cozone variant experience the largest intensities of backstresses near the twin boundary and highest stresses ahead of the twin tip at  $\omega_{opp}$ . The formation of another twin in  $\omega_{opp}$  is, therefore, likely to be of the same variant as the initial variant or its cozone variant (V2 and V2a in this case). If a second twin of the same V2 variant were to form at  $\omega_{opp}$ , the impinging twin would appear to propagate straight "across" the precipitate. On the other hand, if the variant of this second twin is the cozone variant V2a, the twin would seem to kink. Such a structure associated with twin/precipitate junctions has been observed experimentally and referred to as a zig-zagged chain or quilt-like structure [35]. Interestingly, a stress concentration has developed on the side of the twin/precipitate junction where the twin and precipitate intersect at an obtuse angle, at  $\omega_{obtuse}$ . Analysis of the TRSS in this region finds them to be positive and heightened above the average stress in the grain. Further, in the  $\omega_{\it obtuse}$  region, the other variants exhibit higher TRSS compared to the impinging twin and its cozone variant, suggesting that a variant other than V2 or V2a could emanate from the impingement site. These calculations suggest that the interaction between a single impinging twin and a precipitate can trigger the development of other twin variants on both sides of the precipitate, aiding in the development of a complex 3D twin network structure.

#### 3.3. Effect of precipitate width on multiple twin formation

Prior work had discussed the importance of the twin thickness relative to the precipitate length [9], but calculations of the TRSS fields

indicates that the thickness of the precipitate,  $t_P$ , should also be important. By comparing Fig. 1b and c, we observe a shielding effect on the TRSS for the twin (V2) in  $\omega_{opp}$  provided by the precipitate. It is the result of the elastically deforming rigid precipitate resisting the shear of the impinging twin and limiting the development of stress concentrations in the matrix on the other side of the precipitate. The extent of shielding is related to precipitate thickness  $t_P$ .

To examine the effect of  $t_p$ , we study the local driving stresses on either the opposing side in the line of twinning shear, in  $\omega_{opp}$ , or the same side as the twin/precipitate junction, in  $\omega_{obtuse}$ . These are the two sites where the twin is most likely to form after impinging the precipitate. We carried out a series of twin-precipitate interaction calculations for various precipitate thicknesses ranging from 0.14 to four times the thickness of the twin,  $t_t$ . Fig. 3 shows the variation in the averaged TRSS in  $\omega_{opp}$  (solid lines) and in  $\omega_{obtuse}$  (dashed lines) with varying  $t_p/t_t$ . The TRSS is averaged in a quarter circle region in  $\omega_{opp}$  and in a conical region in  $\omega_{obtuse}$ , as schematically shown in the Fig. 3 inset. The values of the primary twin variant (V2) and its covariant (V2a) are marked in black and purple, respectively. Within both  $\omega_{obtuse}$  and  $\omega_{opp}$ , the TRSS for the primary and cozone variant have similar values, within 5 MPa of each other. The TRSS values of all the other variants are nearly identical (within 5 MPa of each other), and thus, are averaged together and shown in red.

The results in Fig. 3 show that as the relative twin thickness increases beyond the precipitate thickness (i.e.,  $t_p/t_t < 1.0$ ), then the twin is more likely to reform on the other side of the precipitate, and the precipitate has less shielding power. The average TRSS for V2 and V2a in  $\omega_{opp}$  are higher than the average TRSS of all the variants in  $\omega_{obtuse}$  when  $t_p/t_t < 1.0$ . Furthermore, the average TRSS values for the V2 and V2a variants range from about 75–110 MPa and are higher than the average TRSS of all the other variants by about 30 MPa in this range, indicating that

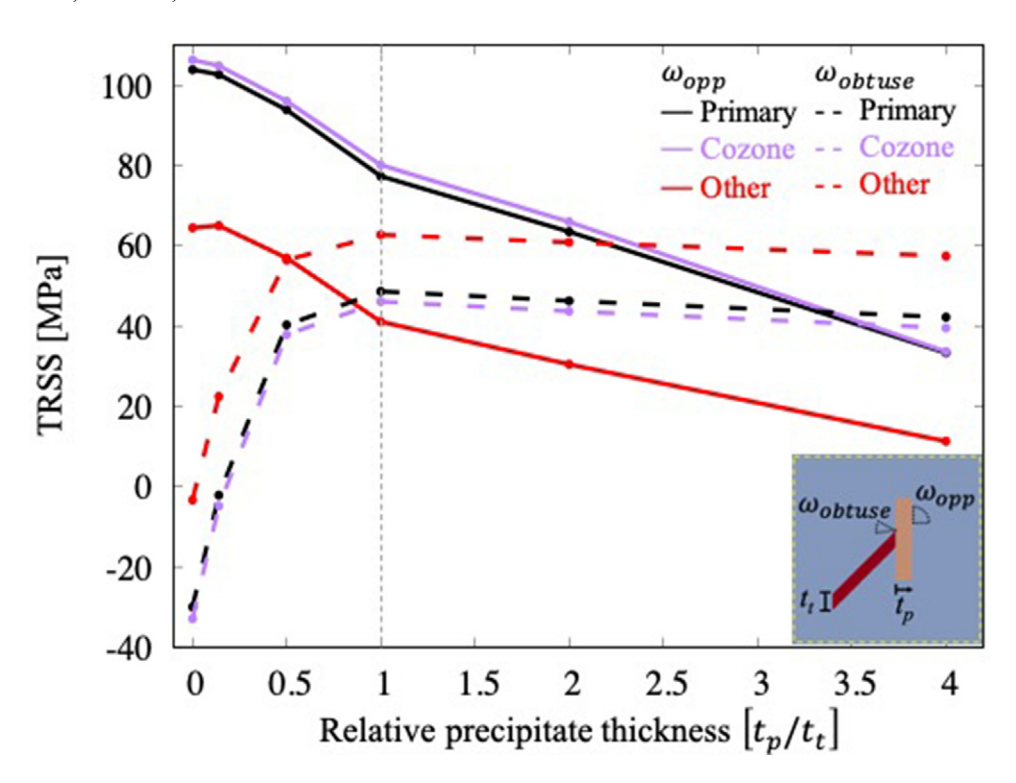


**Fig. 3.** The change in average TRSS taken in  $\omega_{obtuse}$  and  $\omega_{opp}$  with the precipitate thickness,  $t_P$ , normalized by the twin thickness  $t_l$ . The regions  $\omega_{obtuse}$  and  $\omega_{opp}$  are illustrated in the figure inset

a new twin would preferably form in  $\omega_{opp}$  rather than  $\omega_{obtuse}$  and would likely to be the same variant or the cozone variant as the impinging twin. In appearance, the twin would seems to "cross" the precipitate, although it is more like "hopping" over the precipitate, since the precipitate itself does not twin [9,40]. This scenario is similar to the apparent crossing reported in studies of twin-twin interactions [40,50].

Fig. 3 indicates the reverse trend for wider precipitates, as  $t_n/t_t$  increases above unity. As the relative twin thickness decreases further below the precipitate thickness the impinging twin is more likely to "rebound" from the precipitate, producing another variant on the same side as the twin/precipitate junction. When  $t_p/t_t$  becomes greater than or equal to two, the average TRSS of V2 and V2a in  $\omega_{opp}$  and the average TRSS of all other variants in  $\omega_{obtuse}$  are about equal, implying that nucleation on either site is equally likely. In contrast with  $\omega_{opp}$ , in  $\omega_{obtuse}$  the average TRSS for the primary twin and its cozone variant are lower than the other twin variants by about 15 MPa. Here, instead, the twin variants other than the primary variant and its cozone would be favored. In actuality, since the thicknesses of basal precipitates rarely exceed 50 nm [11,48,51] and the thickness of newly propagating twins near the twin tip are usually larger [35], it is expected that a twin nucleation would occur in  $\omega_{opp}$ . The nucleation of a twin on the obtuse angle side is also consistent with previous reports of twin-grain boundary interactions [52].

## 3.4. Staggered twin chain formation

The highly stressed region on the side of the precipitate opposite from the twin tip is extensive, being several times the twin thickness in length, making the exact location of the twin nucleation site difficult to observe. We examine the TRSS along a line Z' in the parent matrix of the precipitate/matrix boundary opposite from the twin/precipitate interaction site, seen in the Fig. 4a inset. In Fig. 4a, the vertical axis represents the position along Z' normalized by  $t_t$ , where Z' is centered along the line of twin shear. We observe that the location of the peak TRSS is offset from the line of twin shear by  $0.41t_t$ . In the example shown in the figure inset, the precipitate thickness equals the twin thickness. Repeating the calculation for other sizes of precipitates reveals that the location of peak TRSS varies with the precipitate thickness. Fig. 4b presents the offset position of the maximum TRSS for various precipitate thicknesses,

normalized by  $t_t$ . For reference, the normalized peak TRSS position for a precipitate free case is presented in dashed lines, measured at distances from twin tip equal to the various precipitate thickness studied here. Even without the precipitate (i.e.,  $t_p/t_t=0$ ), the maximum TRSS at the twin front is not directly aligned with the twin shear direction. Instead, it is offset from the line of shear by  $0.45t_t$ . It draws closer to the line of shear at further distances away from the twin tip, eventually reaching it at distances exceeding  $2t_t$ . The presence of the precipitate extends the peak offset, suggesting that the location where an outgoing twin would be likely to form on the other side of the precipitate would be misaligned from line of shear from the incoming twin. The degree of misalignment increases with decreasing  $t_p$ .

If the primary twin variant is nucleated at the offset location, the twin may appear to "cross" the precipitate and the microstructure may develop a series of staggered twin chains disrupted by precipitates. In Fig. 4c, an enlarged partial Precision Electron Diffraction (PED) micrograph taken from Fig. 1(d) of Xie et al. [35] exhibits staggered twin chains in Mg-9Al that support these findings. The present numerical results are consistent with other experimental reports of twin-precipitate interactions as well, where staggered twin structures have been observed in microscopy [9,23].

Since the TRSS fields of the primary twin and its cozone variant are nearly identical, the outgoing twin can be the same variant as the primary twin or its cozone variant or possibly both. The ability to nucleate either variant may lead to the development of the complex network structure of twins in a series of events. First, the nucleation of a few initial twins can propagate and interact with precipitates, inducing subsequent twins to nucleate. The subsequent twin can be the same variant, resulting in long twin chains. On the other hand, the cozone variant can nucleate, resulting in zig-zagged twin structures like the one seen in the green circle in Fig. 4c [35]. This series of event could be responsible for the development of profuse interconnected twinned structures, rather than the independent nucleation of many individual twins.

# 3.5. Effect of precipitates on twin thickening

We see in Fig. 1b and c that backstresses develop along the twin boundary. Here the backstress at a given point refers specifically to the difference between the TRSS before and after the twin developed.

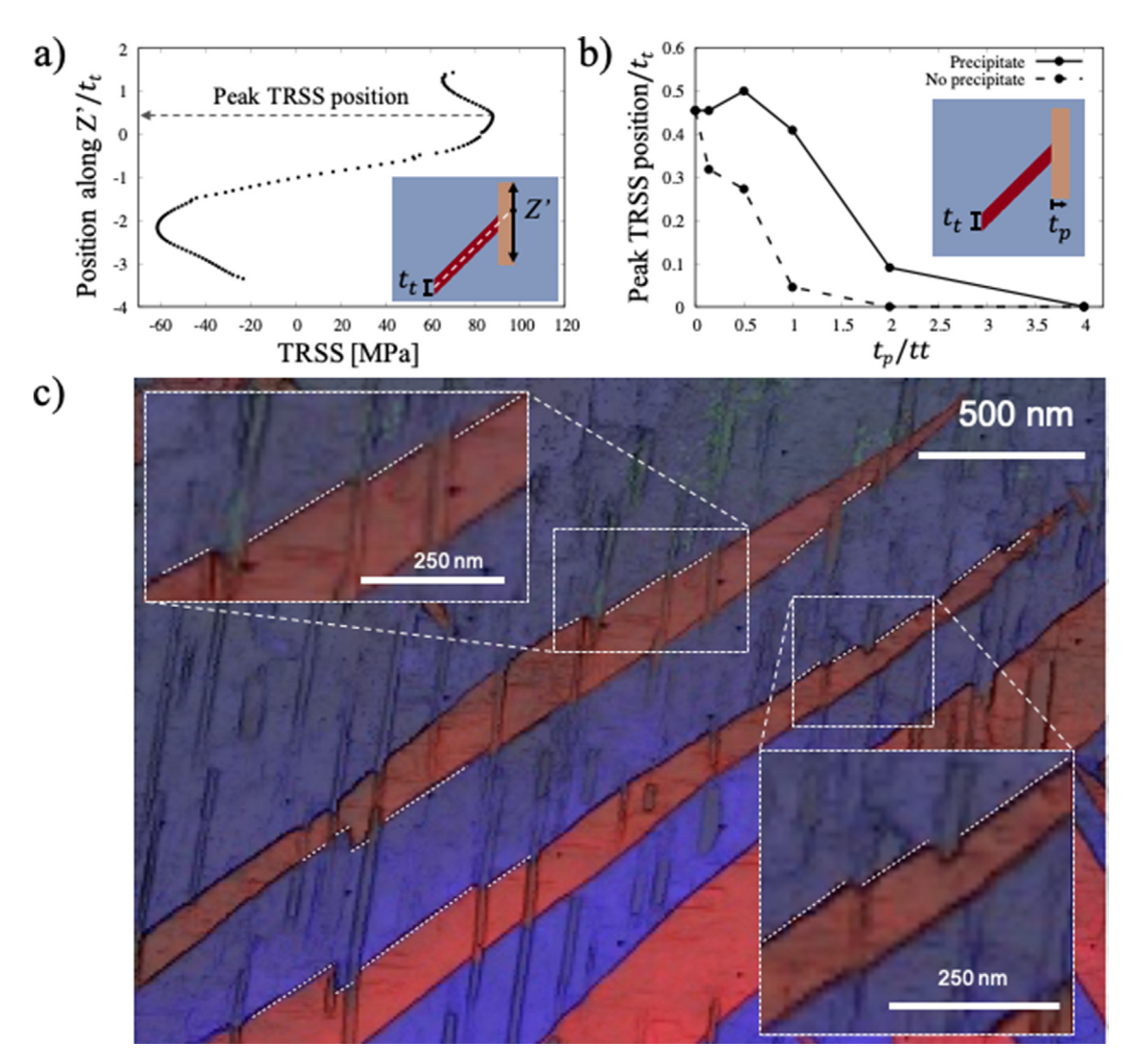


Fig. 4. (a) TRSS profile measured along Z' normalized by the twin thickness. Z' lies in the parent matrix along the precipitate-matrix boundary opposite from the impinging twin tip and is centered along the line of twin shear, as shown in the figure inset. Here, the precipitate thickness is equal the twin thickness. The figure shows that the peak TRSS is vertically offset from the line of twin shear. (b) The normalized offset of the peak TRSS for various precipitate thicknesses is shown in solid lines. The dashed line shows the normalized offset of the peak TRSS for a precipitate-free case measured along vertical lines from twin tip. (c) Precision Electron Diffraction (PED) micrograph of Mg-9Al micropillar sample exemplifying some adjacent twin boundaries that are offset from each other, forming staggered twin formations (highlighted by white dashed lines). The green circle shows an example of cozone twin variants formation at the precipitate interaction site. The micrograph was adopted and modified from Fig. 1(d) of Xie et al. [35] with permission from Elsevier.

Particularly when they are negative, they represent an anti-twinning stress. Because these backstresses can be strong in the vicinity of the twin boundaries, thickening of the twin, by twin boundary migration is not favored [21,53,54]. Twin boundary migration would require sufficiently high applied stresses and would be favored in the event that propagation at the twin-tip has been blunted due to obstacles, like precipitates and grain boundaries.

To study the effect of precipitates on twin boundary migration, in Fig. 5 we show the volumetric average of TRSS in the twin plotted as a function of normalized distance,  $d/t_{\rm t}$ , moving away from the impinging twin tip, see figure inset. For comparison, the TRSS profile for the precipitate-free case presented in black. The results indicate that, as expected, the precipitate causes the backstresses in the twin domain to intensify locally at the twin tip-precipitate interaction site, for instance decreases the TRSS from -128 to -133 MPa.

This precipitate effect on the backstress decreases when moving away from the interaction site, and eventually the TRSS reaches nearly -130 MPa corresponding to the precipitate-free case. This result suggests that twin thickening is restricted by precipitates, a trend that is

consistent with several experimental observations [16,25,29,55]. Prior experimental studies have shown the twin boundary migration is impeded by the presence of the elastically hard precipitates and must bow around the precipitates for the twin to thicken. Most recently, using crystal plasticity-based phase field model, Liu et al. [16] modeled the pinning of a twin boundary at precipitates and captured the increase in stress required for twin thickening. In the present work, a single twintip interaction is investigated rather than the cumulative interactions of twin boundary with multiple precipitates. Both cases, reveal that precipitates restrict twin thickening; however, the twin-tip effect is very localized near the interaction site.

#### 3.6. Effect of impingement site on twin network structure formation

Thus far, we have considered the case in which the twin impinges near or at the center of the precipitate, far away from its edges. The center-impingement scenario is statistically more likely than edge-impingement when the impinging twin is thinner than the length of the precipitate. Yet the chance the twin could hit at the end of the precip-

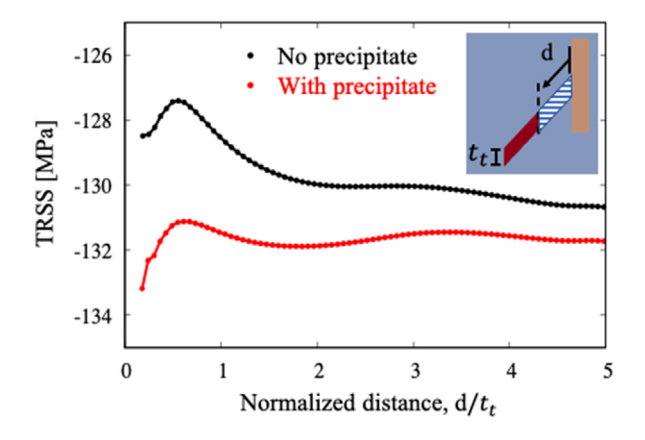


**Fig. 5.** The red lines show the volumetric average TRSS in the twin domain as a function of distance, d, moving away from the twin/precipitate junction, as schematically shown in the figure inset. The black lines correspond to the TRSS with no precipitate present and d is measured from the twin tip. In both cases, the d is normalized by the twin thickness,  $t_i$ .

itate is non-negligible and such an interaction could yield a different outcome since a complex stress state is generated at the end of the precipitate. To study this case, calculations are performed in the event that the twin intersects the precipitate at one of its ends, as illustrated in Fig. 6a. Fig. 6b shows the resulting TRSS field, which is significantly different than that for central impingement shown in Fig. 1c. First, enhanced stresses on the obtuse angle of the twin-precipitate intersection ( $\omega_{obtuse}$ ) are still observed, albeit with a much weaker intensity. Second, the TRSS field ahead of the twin tip ( $\omega_{opp}$ ) appears much stronger, similar to the case in which the twin has not yet impinged on a precipitate (Fig. 1b). Evidently, the precipitate is less effective at shielding when the twin impinges at its end, suggesting that the twin is still able to bypass the precipitate and continue propagating, consistent with TEM observations reported in the literature [9,44].

Given the strong likelihood for continued twin propagation, as seen in Fig. 6b, TRSS fields are calculated for the case when a small embryonic twin has extended past the edge of the precipitate. Fig. 6d presents the TRSS fields, in which three additional stress localizations can be seen, as denoted in Fig. 6c. The first is the enhancement of the stresses at the previous obtuse angle at  $\omega_{obtuse}$ , the second lies directly above the top edge of the precipitate,  $\omega_{top}$ , and the third is the localization that develops where the outgoing twin and precipitate come together at an obtuse angle,  $\omega_{obt*}$ . The two stress concentrations ( $\omega_{top}$  and  $\omega_{obt*}$ ) at the new twin domain provide driving forces for both thickening and propagating. So unlike the parent twin, this new twin can thicken as it propagates, leading to the appearance of relatively large twin domains in the microstructure that "engulf" the precipitate [16,29,55]. Projection of these strong stress concentrations onto the other variants finds that the cozone and primary variant TRSS fields are nearly identical. Therefore, any of these three localized regions could just as likely form

In addition to twin impingement at the upper edge, twins may also impinge on the lower edge of the precipitate, as shown in Fig. 6e. Again, the strong driving stresses ahead of the twin tip and not significantly reduced by the precipitate and it can be expected that the twin may continue propagating unhindered, as shown in Fig. 6g. The respective TRSS fields that arise from bottom edge impingement and the extension of the twin past the precipitate are shown in Fig. 6f and Fig. 6h, respectively. Similarly to upper edge impingement, three additional stress concentrations can be observed in  $\omega_{obtuse}$ ,  $\omega_{bot}$ , and  $\omega_{obt*}$ . Here, however, the stress concentrations are less severe due to the relatively smaller outgoing twin domain. It is expected that as the twin continues propagating forward, these three stress localizations would continue to strengthen acting as twin nucleation sites, similarly to the upper edge impingement case.

The development of additional stress localizations at  $\omega_{top},~\omega_{bot}$  or  $\omega_{obt*}$  act as sites where subsequent twins can propagate to form a network structure. This scenario is consistent with some signatures highlighted in circles in the in-plane inverse pole figure (IPF) maps of the deformed AZ91 microstructure in Fig. 7a [35]. To better distinguish between two variants, Fig. 7b shows the same IPF map as Fig. 7a but with a finer orientation spread. The twin variant corresponding to V2\*  $(01\overline{1}2)$   $[0\overline{1}11]$  is magenta, while the one associated with V2a  $(0\overline{1}12)$   $[01\overline{1}1]$ is blue, as seen in Table 1. When closely observing the white circles in this orientation map, we see the situation where cozone lamellae have formed at the ends of precipitates, where the primary twin lamella has impinged on it. In Fig. 7a, the yellow circle captures the continuation of a twin propagation past the edge of the precipitate, going from bottomright to the top-left. Based on the calculations, we suspect that this twin may have nucleated in  $\omega_{obt*}$ , where the outgoing twin and precipitate come together at an obtuse angle. Last, the green circle in Fig. 7a suggests that two parallel twins could have formed near the edge of the precipitate.

#### 3.7. Remarks on twin propagation pathways

In the present work, we consider only the stresses that arise from a single newly formed twin impinging on an elastically deforming precipitate. The evolution of the twin by either migration of the twin boundary or the nucleation of another twin on the other side of the precipitate is an interesting topic and worthy of investigation in a separate work. Currently, there are many unknowns related to the interactions between a single newly propagated twin and a precipitate. No attempt is made here to quantify the nucleation stress of the twin and the barrier required to nucleate a new twin after the initial twin impingement. Such predictions of twin nucleation barriers and detailed kinetic mechanisms of twin nucleation are possible with an atomistic model that takes into consideration defect concentrations and boundary structure [56-59]. Instead, the mesoscale model used here focuses on the events that occur after a twin has formed and predicts the driving stresses produced around an isolated twin/precipitate interaction. The results provide insight into how the twinned microstructure can develop, irrespective of external considerations, such as local defect structure and external forces. Furthermore, the analysis provided can be generalized to other elastically deforming precipitates with similar dimensions to the plate-shaped basal precipitates studied here.

Based on this study, Fig. 8 proposes various twinning pathways that can arise and explain the varied complex twin network structures seen in precipitate-hardened Mg alloys. If the twin impinges near the center of the precipitate, the incident twin is effectively pinned, and four pathways develop as depicted in Fig. 8a. First, the terminated twin may thicken upon further macroscopic loading. Second, a new twin of the same variant can nucleate on the opposite side of the precipitate. Third, a cozone variant can nucleate on the opposite side of the precipitate. Last, a new twin of the cozone variant is likely to form where the twin and precipitate intersect at an obtuse angle. Alternatively, when the twin impinges near the edge of the precipitate, then the precipitate may not effectively block the initial twin, allowing the twin to continue propagating forward, as illustrated in Fig. 8b and c. In this case, our results suggest four possible pathways for both upper edge impingement and lower edge impingement. First, the outgoing twin may be thicker and more blunted than the initial twin due to the additional closely spaced stress localizations that surround incoming twin tip. Second, an additional twin of the same variant may nucleate closely spaced to the outgoing twin on the opposite side of the precipitate. These two outgoing twins may eventually coalesce, leading to the appearance of thicker twin. Third, a twin of the cozone variant may nucleate where the initial twin and the precipitate intersect at an obtuse angle. Last, a twin of another variant may nucleate, again where the outgoing twin and precipitate intersect at an obtuse angle. These twinning pathways are not limited to a single twin/precipitate interaction, but rather, can be ex-

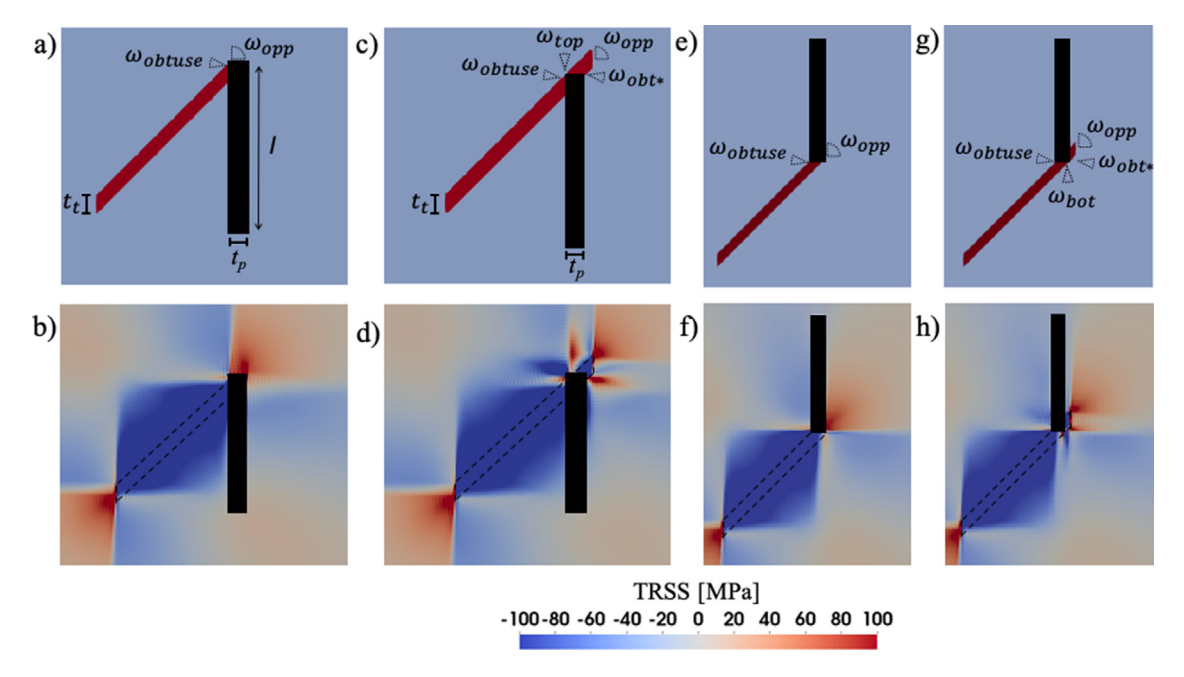


**Fig. 6.** (a) The twin impinging the upper edge of the precipitate. (b) TRSS fields that develop from the twin impinging the upper edge of the precipitate. (c) The twin propagating past the upper edge of the precipitate. (d) TRSS fields that develop from the twin extending past the upper edge of the precipitate. (e) The twin impinging the lower edge of the precipitate. (f) TRSS fields that develop from the twin impinging the lower edge of the precipitate. (g) The twin propagating past the lower edge of the precipitate. (h) TRSS fields that develop from the twin extending past the lower edge of the precipitate.

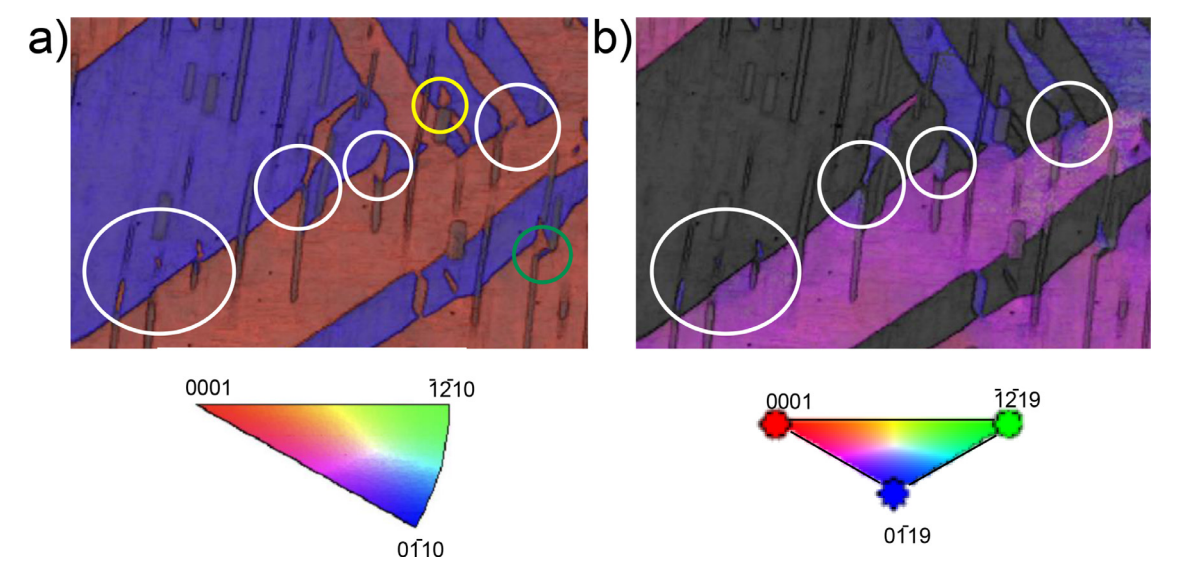


Fig. 7. (a) In-plane inverse pole figure (IPF) map of the compressed Mg-Al alloy. The circles highlight the various twin-tip/precipitate-edge interactions that could lead to the development of a complex network structure of twins. (b) IPF map of the same region using a different color key to distinguish the twin variants. The micrograph was adopted and modified from Fig. 1 of Xie et al. [35] with permission from Elsevier.

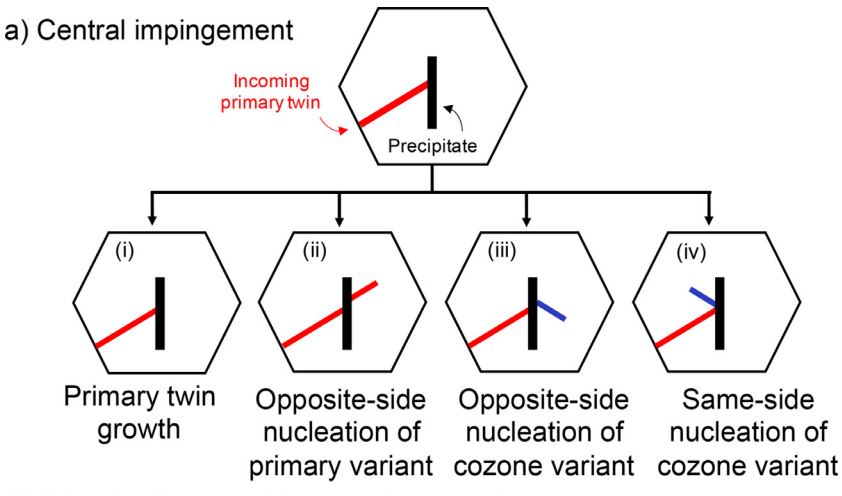
tended to all propagating twins that impinge on a precipitate and twins that nucleate as a result. As shown in Fig. 3, relatively high levels of TRSS in  $\omega_{opp}$ , ranging from 70–110 MPa, can arise solely from the formation of the twin itself, excluding external loads. Consequently, the addition of favorable external loads (i.e., an externally imposed loading direction with respect to the grain orientation that would give positive resolved shear stress for twinning) could further support these conclusions. It is through a cascade of self-catalytic twin propagation and twintip/precipitate interaction events that can lead to the development of twin network structures.

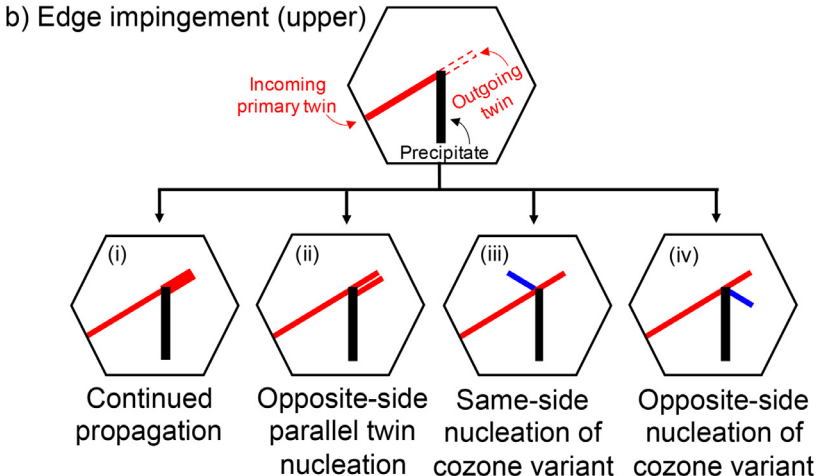
In general, our findings support that basal precipitates that are thicker, in the c-direction of the parent matrix, are more effective at reducing twinning. This is due to the greater shielding effect provided by the precipitate that blocks the driving stress to nucleate another twin

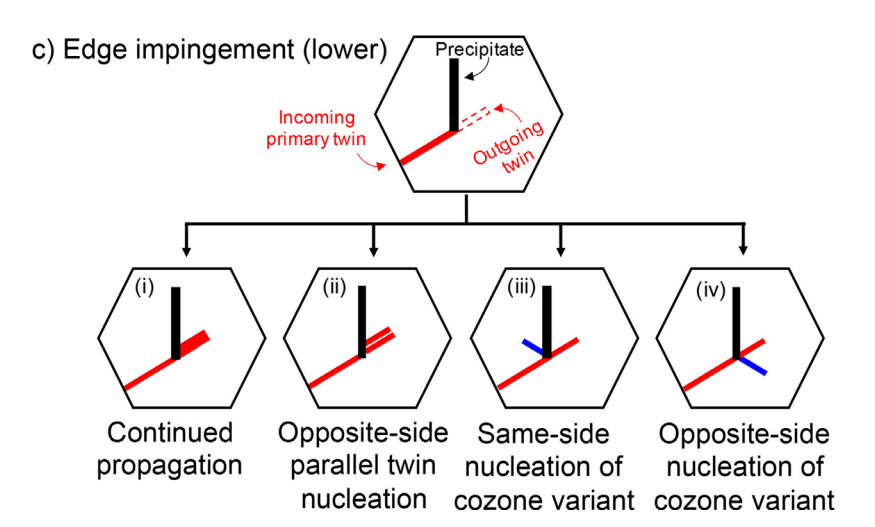
in  $\omega_{opp}$ . The ability to reduce the number of twins by increasing precipitate thickness could potentially be achieved through careful alloying and heat treatment. Furthermore, longer basal precipitates, in the basal plane, can also greatly reduce twinning. This is because, for a given twin volume fraction, smaller precipitates provide more edge interaction sites, increasing the likelihood for twin-tip/precipitate-edge interactions, which can result in multiple high TRSS "hotspots" where new twins can nucleate.

## 4. Summary

In this study, we use a full-field EVP-FFT model to study the effects of twin-tip/precipitate interactions and the influence of these effects on the development of a twinned microstructure. Although often over-







looked, twin-tip propagation is an important stage to consider because the microstructure undergoes significant and rapid changes that will ultimately influence the final twin structures. We focus the analysis on a  $\{10\bar{1}2\}$  tensile twin interactions with plate-shaped basal precipitates in AZ91 Mg alloy. It is understood that twin-tip propagation occurs rapidly until the twin-tip is arrested by an obstacle (e.g., precipitates) or by a grain boundary. However, it is unclear what happens next and why. By simulating an isolated impingement of the twin on a precipitate, we are able to identify for the first time how twin development may continue and the microstructural parameters that influence this.

Fig. 8. a.) Schematic of the twinning pathways that occur after the twin (red) impinges on the precipitate (black). (a) If the twin impinges near the center of a precipitate it is blocked, then to accommodate more strain: (i) the impinging twin can thicken, (ii) a new twin of the same variant (red) can nucleate on the opposite side, likely offset from the twin/precipitate junction, (iii) a cozone variant twin (blue) can nucleate on the opposite side of the precipitate, or (iv) a cozone variant twin can nucleate at the twin/precipitate junction on the side where the twin and precipitate meet at an obtuse angle. (b) If the twin impinges near the upper edge of the precipitate, the twin may continue to propagate forward. As a result: (i) a thicker outgoing twin that is more blunted than the original one. (ii) two parallel twins of the same variant as the primary twin can nucleate, (iii) a cozone variant can nucleate above the top edge of the precipitate, or (iv) a cozone variant twin can nucleate where the outgoing twin and precipitate meet at an obtuse angle. (c) If the twin impinges near the lower edge of the precipitate, the twin may continue to propagate forward. As a result: (i) a thicker outgoing twin that is more blunted than the original one. (ii) two parallel twins of the same variant as the primary twin can nucleate, (iii) a cozone variant can nucleate above the bottom edge of the precipitate, or (iv) a cozone variant twin can nucleate where the outgoing twin and precipitate meet at an obtuse angle.

We find that the precipitate size and the twin tip-precipitate interaction site are important in determining how effective the precipitate is at blocking twin propagation, which twin variants can nucleate, and where new twins can nucleate. In most cases, it is expected that the new twins would tend to nucleate in  $\omega_{opp}$ , opposite form the twin impingement site, where the TRSS localizations are higher. However, for thicker precipitates, the shielding effect is greater, reducing the propensity for a new twin to nucleate in  $\omega_{opp}$  while simultaneously increasing the propensity for twins to nucleate in  $\omega_{obtuse}$ , where the twin and precipitate come together at an obtuse angle. For relatively thick precipitates,  $t_p/t_t > 2$ ,

the driving stresses that aid twin nucleation in  $\omega_{opp}$  and  $\omega_{obtuse}$  become comparable and thus nucleation at either site is equally likely.

The site where the twin impinges on the precipitate can greatly influence subsequent twin development. When a twin impinges near the center of precipitates, the incoming twin is effectively blocked by the precipitates and instead of continued propagation, new twins can nucleate in  $\omega_{obtuse}$  and  $\omega_{opp}$  in order to accommodate strain instead. It is also possible for the twin to impinge near the edge of the precipitate. In this case, the propagation of the incoming twin is not significantly blocked, and incoming twin can continue. The TRSS fields that develop in the matrix after the initial twin propagates past the edge of the precipitate are unique and offer additional twin nucleation sites ( $\omega_{abtuse}$ ,  $\omega_{top}$ , and  $\omega_{obt*}$ ) where the stresses are enhanced and localized. In both cases, the interaction between the twin and precipitates results in the possible multiplication of twin bodies throughout the microstructure. Additionally, twin thickening is also possible albeit considerably more difficult due to the high backstresses in the twin and near the twin boundaries that resist thickening (Eqs. (1)-(4)).

## **Declaration of Competing Interest**

The authors declare no conflict of interest.

#### Acknowledgements

B.L. acknowledges the financial support from the U.S. Department of Defense National Defense Science and Engineering Graduate Fellowship (NDSEG) program. M.A.K. acknowledges the financial support from the U.S. Department of Energy, Office of Basic Energy Sciences (OBES) FWP-06SCPE401. K.Y.X. would like to acknowledge the support from the Los Alamos National Laboratory Fellowship Program initiated at Texas A&M University and Texas A&M Experimental Station. I.J.B. acknowledges financial support from the National Science Foundation Designing Materials to Revolutionize and Engineer our Future (DMREF) program (NSF CMMI-1729887).

#### References

- [1] B.L. Mordike, T. Ebert, Magnesium properties applications potential, Mater. Sci. Eng. A 302 (2001) 37–45, doi:10.1016/S0921-5093(00)01351-4.
- [2] T.M. Pollock, Weight loss with magnesium alloys, Science 328 (2010) 986–987, doi:10.1126/science.1182848.
- [3] D. Zhao, X. Ma, A. Srivastava, G. Turner, I. Karaman, K.Y. Xie, Significant disparity of non-basal dislocation activities in hot-rolled highly-textured Mg and Mg-3Al-1Zn alloy under tension, Acta Mater. 207 (2021) 116691, doi:10.1016/j.actamat.2021.116691.
- [4] J.J. Bhattacharyya, S.R. Kada, M.R. Barnett, S.R. Agnew, Crystal plasticity and in-situ diffraction-based determination of the dislocation strengthening and loadsharing effects of precipitates in Mg alloy, AZ91, Materialia 6 (2019) 100308, doi:10.1016/j.mtla.2019.100308.
- [5] M.K. Singh, Application of steel automotive industry, Int. J. Emerg. Technol. Adv. Eng. 6 (2016) 246–253.
- [6] J.G. Kaufman, Mechanical properties aluminum 6000 series, in: Properties of Aluminum Alloys, ASM International Technical Books Committee, 1999, pp. 162–198.
- [7] T. Nakata, C. Xu, R. Ajima, K. Shimizu, S. Hanaki, T.T. Sasaki, L. Ma, K. Hono, S. Kamado, Strong and ductile age-hardening Mg-Al-Ca-Mn alloy that can be extruded as fast as aluminum alloys, Acta Mater. 130 (2017) 261–270, doi:10.1016/j.actamat.2017.03.046.
- [8] I.M. Baghni, W. Yinshun, L. Jiuqing, D. Cuiwei, Z. Wei, Mechanical properties and potential applications of magnesium alloys, Trans. Nonferrous Met. Soc. China (2003).
- [9] M.A. Gharghouri, G.C. Weatherly, J.D. Embury, The interaction of twins and precipitates in a Mg-7.7 at.% Al alloy, Philos. Mag. A 78 (1998) 1137–1149 Phys. Condens. Matter, Struct. Defects Mech. Prop, doi:10.1080/01418619808239980.
- [10] S.R. Agnew, R.P. Mulay, F.J. Polesak, C.A. Calhoun, J.J. Bhattacharyya, B. Clausen, In situ neutron diffraction and polycrystal plasticity modeling of a Mg-Y-Nd-Zr alloy: effects of precipitation on individual deformation mechanisms, Acta Mater. 61 (2013) 3769–3780, doi:10.1016/j.actamat.2013.03.010.
- [11] J.D. Robson, N. Stanford, M.R. Barnett, Effect of precipitate shape on slip and twinning in magnesium alloys, Acta Mater. 59 (2011) 1945–1956, doi:10.1016/j.actamat.2010.11.060.
- [12] J.D. Robson, N. Stanford, M.R. Barnett, Effect of precipitate shape and habit on mechanical asymmetry in magnesium alloys, Metall. Mater. Trans. A 44 (2013) 2984–2995 Phys. Metall. Mater. Sci., doi:10.1007/s11661-012-1466-0.

[13] C.Y. Wang, C.M. Cepeda-Jiménez, M.T. Pérez-Prado, Dislocation-particle interactions in magnesium alloys, Acta Mater. 194 (2020) 190–206, doi:10.1016/j.actamat.2020.04.055.

- [14] J.F. Nie, Effects of precipitate shape and orientation on dispersion strengthening in magnesium alloys, Scr. Mater. 48 (2003) 1009–1015, doi:10.1016/S1359-6462(02)00497-9.
- [15] F. Wang, J.J. Bhattacharyya, S.R. Agnew, Effect of precipitate shape and orientation on Orowan strengthening of non-basal slip modes in hexagonal crystals, application to magnesium alloys, Mater. Sci. Eng. A 666 (2016) 114–122, doi:10.1016/j.msea.2016.04.056.
- [16] C. Liu, P. Shanthraj, J.D. Robson, M. Diehl, S. Dong, J. Dong, W. Ding, D. Raabe, On the interaction of precipitates and tensile twins in magnesium alloys, Acta Mater. 178 (2019) 146–162, doi:10.1016/j.actamat.2019.07.046.
- [17] J.J. Bhattacharyya, F. Wang, N. Stanford, S.R. Agnew, Slip mode dependency of dislocation shearing and looping of precipitates in Mg alloy WE43, Acta Mater. 146 (2018) 55–62, doi:10.1016/j.actamat.2017.12.043.
- [18] J. Jiang, S. Ni, H. Yan, N. Yan, M. Song, (c + a) dislocations shearing (0001)α plate precipitates in an Mg-Zn-Mn alloy, Scr. Mater. 170 (2019) 24–28, doi:10.1016/j.scriptamat.2019.05.022.
- [19] E.L.S. Solomon, E.A. Marquis, Deformation behavior of b' and b'" precipitates in Mg-RE alloys, Mater. Lett. 216 (2018) 67–69, doi:10.1016/j.matlet.2017.12.149.
- [20] M.H. Yoo, J.K. Lee, Deformation twinning in h.c.p. metals and alloys, Philos. Mag. A 63 (1991) 987–1000 Phys. Condens. Matter, Struct. Defects Mech. Prop, doi:10.1080/01418619108213931.
- [21] M. Arul Kumar, A.K. Kanjarla, S.R. Niezgoda, R.A. Lebensohn, C.N. Tomé, Numerical study of the stress state of a deformation twin in magnesium, Acta Mater. 84 (2015) 349–358, doi:10.1016/j.actamat.2014.10.048.
- [22] I.J. Beyerlein, L. Capolungo, P.E. Marshall, R.J. McCabe, C.N. Tome, Statistical analyses of deformation twinning in magnesium, Philos. Mag. 90 (2010) 2161–2190, doi:10.1080/14786431003630835.
- [23] N. Stanford, M.R. Barnett, Effect of particles on the formation of deformation twins in a magnesium-based alloy, Mater. Sci. Eng. A 516 (2009) 226–234, doi:10.1016/j.msea.2009.04.001.
- [24] J. Jain, P. Cizek, W.J. Poole, M.R. Barnett, The role of back stress caused by precipitates on {101-2} twinning in a Mg-6Zn alloy, Mater. Sci. Eng. A 647 (2015) 66–73, doi:10.1016/j.msea.2015.08.091.
- [25] J.D. Robson, N. Stanford, M.R. Barnett, Effect of particles in promoting twin nucleation in a Mg-5 wt.% Zn alloy, Scr. Mater. 63 (2010) 823–826, doi:10.1016/j.scriptamat.2010.06.026.
- [26] J. Jain, W.J. Poole, C.W. Sinclair, M.A. Gharghouri, Reducing the tension compression yield asymmetry in a Mg –8Al –0.5Zn alloy via precipitation, Scr. Mater. 62 (2010) 301–304, doi:10.1016/j.scriptamat.2009.11.024.
- [27] P. Hidalgo-Manrique, J.D. Robson, Interaction between precipitate basal plates and tensile twins in magnesium alloys, Metall. Mater. Trans. A 50 (2019) 3855–3867 Phys. Metall. Mater. Sci., doi:10.1007/s11661-019-05301-1.
- [28] B. Zhang, C. Yang, Y. Sun, J. Li, F. Liu, Effects of AlN reinforcement particles on the twinning nucleation and growth in AZ91 alloy, Mater. Today Commun. 24 (2020) 101023. doi:10.1016/j.mtcomm.2020.101023.
- [29] X.Z. Tang, Y.F. Guo, The engulfment of precipitate by extension twinning in Mg-Al alloy, Scr. Mater. 188 (2020) 195–199, doi:10.1016/j.scriptamat.2020.07.020.
- [30] H. Fan, Y. Zhu, J.A. El-Awady, D. Raabe, Precipitation hardening effects on extension twinning in magnesium alloys, Int. J. Plast. 106 (2018) 186–202, doi:10.1016/j.ijplas.2018.03.008.
- [31] D.J. Bacon, U.F. Kocks, R.O. Scattergood, The effect of dislocation self-interaction on the orowan stress, Philos. Mag. 28 (1973) 1241–1263, doi:10.1080/14786437308227997.
- [32] M.R. Barnett, Twinning super dislocations to help understand strength, in: Magnesium Technology, 2017, The Minerals, Metals & Material Society (TMS), 2017, pp. 143–145.
- [33] M.R. Barnett, H. Wang, Interaction between propagating twins and non-shearable precipitates in magnesium alloys, in: Proceedings of the TMS Magnesium Technology Symposium, 2018, pp. 365–367. TMS.
- [34] F. Siska, L. Stratil, J. Cizek, T. Guo, M. Barnett, Numerical analysis of twin-precipitate interactions in magnesium alloys, Acta Mater. 202 (2021) 80–87, doi:10.1016/j.actamat.2020.10.053.
- [35] K.Y. Xie, D. Zhao, B. Leu, X. Ma, Q. Jiao, J.A. El-Awady, T.P. Weihs, I.J. Beyerlein, M.A. Kumar, Understanding the interaction of extension twinning and basal-plate precipitates in Mg-9Al using precession electron diffraction, Materialia (2021) 15, doi:10.1016/j.mtla.2021.101044.
- [36] J.P. Zhou, D.S. Zhao, R.H. Wang, Z.F. Sun, J.B. Wang, J.N. Gui, O. Zheng, In situ observation of ageing process and new morphologies of continuous precipitates in AZ91 magnesium alloy, Mater. Lett. 61 (2007) 4707–4710, doi:10.1016/j.matlet.2007.03.013.
- [37] M. Arul Kumar, I.J. Beyerlein, C.N. Tomé, Effect of local stress fields on twin characteristics in HCP metals, Acta Mater. 116 (2016) 143–154, doi:10.1016/j.actamat.2016.06.042.
- [38] R.A. Lebensohn, A.K. Kanjarla, P. Eisenlohr, An elasto-viscoplastic formulation based on fast Fourier transforms for the prediction of micromechanical fields in polycrystalline materials, Int. J. Plast. 32–33 (2012) 59–69, doi:10.1016/j.ijplas.2011.12.005.
- [39] M. Arul Kumar, I.J. Beyerlein, R.J. McCabe, C.N. Tomé, Grain neighbour effects on twin transmission in hexagonal close-packed materials, Nat. Commun. 7 (2016) 13826, doi:10.1038/ncomms13826.
- [40] J.W. Zhang, B. Leu, M.A. Kumar, I.J. Beyerlein, W.Z. Han, Twin hopping in nanolayered Zr-2.5Nb, Mater. Res. Lett. 8 (2020) 307–313, doi:10.1080/21663831.2020.1755902.

- [41] M. Arul Kumar, B. Leu, P. Rottmann, I.J. Beyerlein, Characterization of Staggered Twin Formation in HCP Magnesium, in: Magnesium Technology, The Minerals, Metals & Material Society (TMS), 2019, pp. 207–213, doi:10.1007/978-3-030-05789-3 17.
- [42] D. Duly, M.C. Cheynet, Y. Brechet, Morphology and chemical nanoanalysis of discontinuous precipitation in MgAl alloys-I. Regular growth, Acta Metall. Mater. 42 (1994) 3843–3854. doi:10.1016/0956-7151(94)90450-2.
- [43] M.X. Zhang, P.M. Kelly, Crystallography of Mg17Al12 precipitates in AZ91D alloy, Scr. Mater. 48 (2003) 647–652, doi:10.1016/S1359-6462(02)00555-9.
- [44] J.D. Robson, M.R. Barnett, The effect of precipitates on twinning in magnesium alloys, Adv. Eng. Mater. 21 (2019) 1–10, doi:10.1002/adem.201800460.
- [45] G. Simmons, H. Wang, Single Crystal Elastic Constants and Calculated Aggregate Progress, 2nd ed., The M.I.T. Press, 1965.
- [46] N. Wang, W.Y. Yu, B.Y. Tang, L.M. Peng, W.J. Ding, Structural and mechanical properties of Mg17Al12 and Mg24Y5 from first-principles calculations, J. Phys. D Appl. Phys. (2008) 41, doi:10.1088/0022-3727/41/19/195408.
- [47] J.D. Robson, The effect of internal stresses due to precipitates on twin growth in magnesium, Acta Mater. 121 (2016) 277–287, doi:10.1016/j.actamat.2016.09.022.
- [48] X. Ma, Q. Jiao, L.J. Kecskes, J.A. El-Awady, T.P. Weihs, Effect of basal precipitates on extension twinning and pyramidal slip: a micro-mechanical and electron microscopy study of a Mg-Al binary alloy, Acta Mater. 189 (2020) 35–46, doi:10.1016/j.actamat.2020.02.037.
- [49] S. Si, J. Wu, I.P. Jones, Y.L. Chiu, Influence of precipitates on basal dislocation slip and twinning in AZ91 micro-pillars, Philos. Mag. (2020) 2949–2971, doi:10.1080/14786435.2020.1802077.
- [50] Q. Yu, J. Wang, Y. Jiang, R.J. McCabe, N. Li, C.N. Tomé, Twin-twin interactions in magnesium, Acta Mater. 77 (2014) 28–42, doi:10.1016/j.actamat.2014. 05.030.

[51] N. Stanford, J. Geng, Y.B. Chun, C.H.J. Davies, J.F. Nie, M.R. Barnett, Effect of plate-shaped particle distributions on the deformation behaviour of magnesium alloy AZ91 in tension and compression, Acta Mater. 60 (2012) 218–228, doi:10.1016/j.actamat.2011.10.001.

- [52] M. Arul Kumar, L. Capolungo, R.J. McCabe, C.N. Tomé, Characterizing the role of adjoining twins at grain boundaries in hexagonal close packed materials, Sci. Rep. 9 (2019) 1–10. doi:10.1038/s41598-019-40615-5.
- [53] Y. Zhu, X. Wu, Perspective on hetero deformation induced (HDI) hardening and backstress, Mater. Res. Lett. 7 (2019) 393–398.
- [54] L. Balogh, S.R. Niezgoda, A.K. Kanjarla, D.W. Brown, B. Clausen, W. Liu, C.N. Tomé, Spatially resolved in situ strain measurements from an interior twinned grain in bulk polycrystalline AZ31 alloy, Acta Mater. 61 (2013) 3612–3620, doi:10.1016/j.actamat.2013.02.048.
- [55] N. Stanford, M.R. Barnett, Solute strengthening of prismatic slip, basal slip and {1012} twinning in Mg and Mg-Zn binary alloys, Int. J. Plast. 47 (2013) 165–181, doi:10.1016/j.ijplas.2013.01.012.
- [56] W.Z. Han, J.S. Carpenter, J. Wang, I.J. Beyerlein, N.A. Mara, Atomic-level study of twin nucleation from face-centered-cubic/body- centered-cubic interfaces in nanolamellar composites, Appl. Phys. Lett. (2012) 100, doi:10.1063/1.3675447.
- [57] J. Wang, I.J. Beyerlein, C.N. Tomé, An atomic and probabilistic perspective on twin nucleation in Mg, Scr. Mater. 63 (2010) 741–746, doi:10.1016/j.scriptamat.2010.01.047.
- [58] S.R. Niezgoda, A.K. Kanjarla, I.J. Beyerlein, C.N. Tomé, Stochastic modeling of twin nucleation in polycrystals: an application in hexagonal close-packed metals, Int. J. Plast. 56 (2014) 119–138, doi:10.1016/j.ijplas.2013.11.005.
- [59] I.J. Beyerlein, C.N. Tomé, A probabilistic twin nucleation model for HCP polycrystalline metals, Proc. R. Soc. A 466 (2010) 2517–2544 Math. Phys. Eng. Sci., doi:10.1098/rspa.2009.0661.